

Proposal for Realizing Quantum Scars in the Tilted 1D Fermi-Hubbard Model

Jean-Yves Desaulès¹, Ana Hudomal^{1,2}, Christopher J. Turner¹ and Zlatko Papić¹

¹*School of Physics and Astronomy, University of Leeds, Leeds LS2 9JT, United Kingdom*

²*Institute of Physics Belgrade, University of Belgrade, 11080 Belgrade, Serbia*



(Received 8 February 2021; revised 9 April 2021; accepted 19 April 2021; published 24 May 2021)

Motivated by recent observations of ergodicity breaking due to Hilbert space fragmentation in 1D Fermi-Hubbard chains with a tilted potential [Scherg *et al.*, [arXiv:2010.12965](https://arxiv.org/abs/2010.12965)], we show that the same system also hosts quantum many-body scars in a regime $U \approx \Delta \gg J$ at electronic filling factor $\nu = 1$. We numerically demonstrate that the scarring phenomenology in this model is similar to other known realizations such as Rydberg atom chains, including persistent dynamical revivals and ergodicity-breaking many-body eigenstates. At the same time, we show that the mechanism of scarring in the Fermi-Hubbard model is different from other examples in the literature: the scars originate from a subgraph, representing a free spin-1 paramagnet, which is weakly connected to the rest of the Hamiltonian's adjacency graph. Our work demonstrates that correlated fermions in tilted optical lattices provide a platform for understanding the interplay of many-body scarring and other forms of ergodicity breaking, such as localization and Hilbert space fragmentation.

DOI: [10.1103/PhysRevLett.126.210601](https://doi.org/10.1103/PhysRevLett.126.210601)

Introduction.—Recently, there has been much interest in understanding how closed many-body quantum systems evolve in time when taken out of their equilibrium state. While many such systems rapidly return to their equilibrium state, in accordance with fundamental principles of quantum statistical mechanics [1], much of recent work has focused on systems that fail to do so as a consequence of ergodicity breaking [2,3], either due to the special mathematical structure known as integrability or very strong disorder which leads to (many-body) localization. Both of these paradigms of behavior are actively investigated in experiments on cold atoms, trapped ions, and superconducting qubits [4–7].

The inability of nonergodic systems to act as heat reservoirs for their smaller parts has been traditionally known to affect the entire spectrum of the system. Recently, however, there has been a flurry of interest in *weak* ergodicity breaking phenomena [8]. The latter refers to the emergence of a dynamically decoupled subspace within the many-body Hilbert space, in general without any underlying symmetry, spanned by ergodicity-breaking eigenstates. This behavior was first theoretically established in the Affleck-Kennedy-Lieb-Tasaki (AKLT) model [9,10], followed by the discovery of similar phenomenology in other nonintegrable lattice models [11–18], models of correlated fermions and bosons [19–25], frustrated magnets [26,27], topological phases of matter [28,29], and periodically driven systems [30–34]. In these examples, the ergodicity-breaking eigenstates are either explicitly embedded into a many-body spectrum via the mechanism due to Shiraishi and Mori [35], or they form a representation of an algebra [36–38].

A well-known example of weak ergodicity breaking in single-particle systems is the phenomenon of quantum scars in chaotic stadium billiards [39]. In this case, the particle's eigenfunctions exhibit anomalous concentration in the vicinity of an unstable periodic orbit in the classical limit $\hbar \rightarrow 0$ [40–42], leading to observable consequences in many physical systems [43–46]. In recent experiments on interacting Rydberg atom arrays [47], weak ergodicity breaking was observed via persistent revivals following the global quench of the system, prompting the name “quantum many-body scarring” [48–50] by analogy with stadium billiards [51,52]. Recently, quantum many-body scarring has been shown to occur in higher dimensions [53–55] and in the presence of certain kinds of perturbations [56–58] including disorder [59].

On the other hand, it has also been shown that ergodicity breaking can occur due to a fracturing of the Hilbert space into dynamically disconnected components [60–63]. This typically occurs by the interplay of local interactions with a higher-moment symmetry such as charge dipole conservation, which nontrivially intertwines spatial and internal symmetries. Recent work [64] has demonstrated that Hilbert space fragmentation can be experimentally realized via a magnetic field gradient applied to the Fermi-Hubbard (FH) model in a 1D optical lattice. Apart from offering a new platform to investigate the link between fragmentation and the so-called Stark many-body localization [65–67], an immediate question presents itself: can the tilted FH model realize quantum many-body scars?

In this Letter, we show that quantum many-body scars arise in the limit $U \approx \Delta \gg J$ in the tilted FH model, and that they can be detected using the quench from a specific

initial state at a different filling factor from the one considered in Ref. [64]. We derive an effective model for this setup, which can be mapped to a spinful generalization of the fractional quantum Hall effect on a thin torus [23], allowing for a practical experimental realization. While the phenomenology of quantum many-body scars is shown to be largely similar to their realization in Rydberg atom systems [47], including in particular an extensive set of eigenstates which violate the eigenstate thermalization hypothesis (ETH) [68,69], the origin of scars is different in the two systems and can be intuitively understood from a graph-theoretic viewpoint.

Large-tilt limit of the FH model.—The 1D FH model is given by the Hamiltonian

$$\hat{H} = \sum_{j,\sigma=\uparrow,\downarrow} -J\hat{c}_{j,\sigma}^\dagger\hat{c}_{j+1,\sigma} + \text{H.c.} + \Delta j\hat{n}_{j,\sigma} + U\sum_j \hat{n}_{j,\uparrow}\hat{n}_{j,\downarrow}, \quad (1)$$

where $\hat{c}_{j,\sigma}^\dagger$ denotes the usual electron creation operator on site j with spin projection σ , $\hat{n}_{j,\sigma} \equiv \hat{c}_{j,\sigma}^\dagger\hat{c}_{j,\sigma}$, J and U are the hopping and on-site interaction terms, respectively. Tilt of the optical lattice is parametrized by Δ , which we take to be spin independent [64]. Note that tilting has the structure of a dipole term, $\sim j\hat{n}_j$. Below we impose open boundary conditions on the model in Eq. (1), and restrict to the electron filling factor $\nu = 1$, i.e., with $N/2$ fermions with spin \uparrow and $N/2$ fermions with spin \downarrow on a chain of N sites (assumed to be even). We also set $J = 1$ for simplicity. We label the Fock states using \uparrow to denote a fermion with spin up and \downarrow with spin down, while 0 stands for an empty site and $\downarrow\downarrow$ denotes a doublon.

We focus on the regime $\Delta \approx U \gg J$. In this case the sum of the dipole moment and the number of doublons is effectively conserved. The dominant contribution to the Hamiltonian (using a Schrieffer-Wolff transformation at first order [70]) is then given by

$$\begin{aligned} \hat{H}_{\text{eff}} = & -J\sum_{j,\sigma}\hat{c}_{j,\sigma}^\dagger\hat{c}_{j+1,\sigma}\hat{n}_{j,\bar{\sigma}}(1 - \hat{n}_{j+1,\bar{\sigma}}) + \text{H.c.} \\ & + (U - \Delta)\sum_j \hat{n}_{j,\uparrow}\hat{n}_{j,\downarrow}. \end{aligned} \quad (2)$$

In this effective Hamiltonian, hopping to the left (which decreases the total dipole moment by 1) is only allowed if it increases the number of doublons by the same amount ($\bar{\sigma}$ denotes opposite spin from σ).

The action of the Hamiltonian Eq. (2) within the $\nu = 1$ sector fragments the Hilbert space beyond the simple conservation of $U + \Delta$. In this work we focus on the largest connected component, which is the one containing the state with alternating \uparrow and \downarrow fermions. In addition to the symmetries of the full model in Eq. (1), i.e., $SU(2)$ spin symmetry and spin reversal [71], the Hamiltonian Eq. (2) projected to the largest sector has an additional symmetry

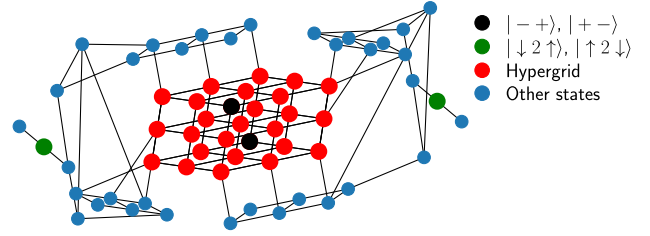


FIG. 1. Adjacency graph of the effective model in Eq. (2) for $N = 6$. Red vertices denote the states belonging to the hypergrid, with the black vertices corresponding to $| - + \rangle$, $| + - \rangle$ states defined in the text. Green vertices are the isolated states $|\downarrow 2\uparrow\rangle$, $|\uparrow 2\downarrow\rangle$ which live on the tails of the graph. For this graph, the hypergrid contains 27 vertices out of 63.

related to spatial inversion and particle-hole exchange [72]. After resolving these symmetries, we find the level statistics parameter $\langle r \rangle$ [73] to be close to 0.53 for all symmetry sectors with large numbers of states ($\gtrsim 10^3$) [72]. From these values which coincide with the Wigner-Dyson statistics [74], we expect the model in Eq. (2) to be chaotic. We next outline an intuitive approach for identifying many-body scars in this model.

Embedded hypergrid subgraph.—A practical diagnostic of quantum many-body scars is the existence of weakly correlated states which undergo robust revivals under quench dynamics, while the majority of other initial states thermalize fast and do not display revivals. In the Rydberg-blockaded chains [47], the reviving Néel state of atoms is the densest configuration compatible with the blockade constraint, and it is an extremal vertex of the Hamiltonian adjacency graph [48]. In this graph each vertex corresponds to a basis state, and two vertices are connected by an edge if the Hamiltonian matrix element between their respective basis states is nonzero. We next show, by examining the adjacency graph of the model in Eq. (2), that we can identify a subgraph, weakly coupled to the rest of the Hilbert space, which contains the reviving initial states and leaves a strong imprint on the scarred eigenstates. This leads to a transparent manifestation of scarring in the original Fock basis, in contrast with Rydberg atoms. In the latter case, the subspace which is weakly coupled to the rest of the Hilbert space has a much more complicated structure, leading to the wave function spreading across the entire adjacency graph [56] before refocusing onto the Néel state.

In Fig. 1 we plot the adjacency graph of the Hamiltonian in Eq. (2) for a small system. For the effective model in Eq. (2), it is possible to gauge away the fermionic minus signs [72], resulting in an unweighted, undirected graph. As the Hamiltonian Eq. (2) (for $U = \Delta$) has no diagonal elements and the spectrum is symmetric around zero, all product states are effectively in the infinite temperature ensemble and are expected to thermalize quickly. As we confirm numerically below, there are two important exceptions.

First, as highlighted in red color in Fig. 1, there is a regular subgraph which has the form of the hypergrid—a Cartesian product of line graphs (in our case, of length 3), i.e., the hypergrid is isomorphic to an adjacency graph of a free spin-1 paramagnet. This mapping can be understood by looking at the state $|\downarrow\uparrow\downarrow\uparrow\downarrow\uparrow\dots\rangle$. Each cell of two sites can take the values $- := \downarrow\uparrow$, $2 := \uparrow\downarrow$ or $+$ $:= \uparrow\uparrow$, leading to a three level system. Note that the configuration $0\uparrow$ is omitted, as doublons can only be formed by hopping to the left. On the other hand, hopping between two neighboring cells will break this mapping and take the system out of the hypergrid subgraph. Inside the hypergrid, we identify two states for which the cell alternates between $-$ and $+$. These are the state $| - + \rangle := | - + - + \dots \rangle = |\downarrow\uparrow\downarrow\uparrow\downarrow\uparrow\downarrow\dots\rangle$ and its spin-inverted partner, $| + - \rangle = | + - + - \dots \rangle := |\uparrow\downarrow\uparrow\downarrow\uparrow\downarrow\uparrow\dots\rangle$. The states $| - + \rangle$ and $| + - \rangle$ for $N = 6$ are shown in black color in Fig. 1. These two states are the only corners of the hypergrid (state with only $+$ and $-$ cells) with no edges going out of it. As we show below, either of these states shows persistent oscillations in quench dynamics, undergoing robust state transfer to their spin-inverted counterpart. While other corners of the hypergrid also show revivals, they are much smaller in amplitude and decay faster due to the leakage out of this substructure. The second example of a reviving state is $|\downarrow 2 \uparrow\rangle := |\downarrow\downarrow\dots\downarrow\uparrow\downarrow\uparrow\dots\rangle$ (and its spin-reversed partner $|\uparrow 2 \downarrow\rangle$), which is situated on a tail-like structure of length 3 (independent of system size) with minimal connectivity to the rest of the Hilbert space (green points in Fig 1). Similar tail-like structures occur in constrained spin models [75].

Many-body scarred dynamics and eigenstates.—Having identified candidate states for revivals, we now scrutinize their quench dynamics using large-scale exact diagonalization simulations of the effective model in Eq. (2). Making use of various symmetries present in the model, we have been able to exactly simulate dynamics for up to $N = 22$ electrons. For convenience, the simulations were performed in the spin representation of the model [72].

Figure 2(a) shows the time dependence of the entanglement entropy $S_{\text{ent}}(t)$ when the system is quenched from various initial product states, such as $| - + \rangle$, $|\downarrow 2 \uparrow\rangle$ and a few randomly chosen product states. S_{ent} is defined as the von Neumann entropy of the reduced density matrix for one half of the chain. In all cases, entropy grows linearly in time, consistent with thermalization of the system. However, the coefficient of linear growth is visibly different for $| - + \rangle$ and $|\downarrow 2 \uparrow\rangle$ states, and it is smaller than that of random states, indicating nonergodic dynamics. The long-time value of the entropy is also different for the $| - + \rangle$ state [72], hinting that the wave function is still not completely spread into the whole Hilbert space. The hallmark of many-body scars is the oscillations superposed on top of the linear growth, as seen in the scarred dynamics in Rydberg atom chains [48]. Rapid

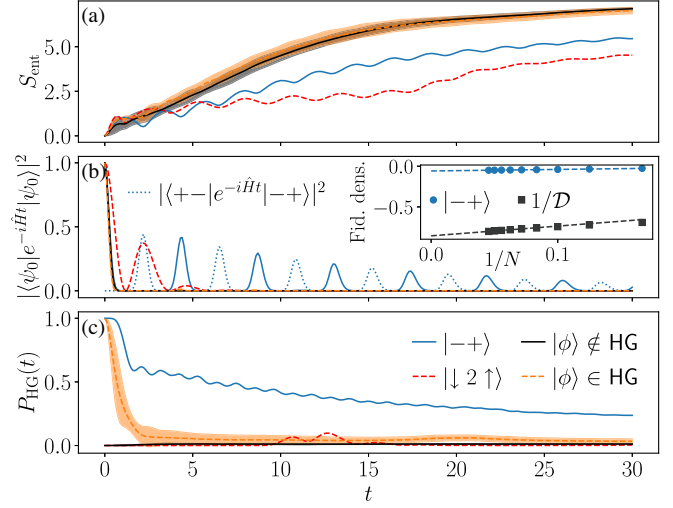


FIG. 2. Dynamics in the effective model Eq. (2) for $N = 18$ for $| - + \rangle$, $|\downarrow 2 \uparrow\rangle$ and randomly chosen initial states. (a) Entanglement entropy S_{ent} for an equal bipartition of the system. Entropy grows linearly in time for all states, consistent with thermalizing dynamics, but it shows oscillations due to many-body scarring. $|\phi\rangle \notin \text{HG}$ and $|\phi\rangle \in \text{HG}$ denote the average over 10 random product states outside or within the hypergrid, respectively, and the shading represents standard deviation. (b) Fidelity dynamics for the same initial states as in (a). Inset shows the finite-size scaling of the fidelity density $1/N \ln |\langle\psi_0|e^{-iHt}|\psi_0\rangle|^2$ at the first revival for $| - + \rangle$ state, demonstrating a value much higher than $1/N \ln(1/D)$ (with D the dimension of the Hilbert space), expected for a random state. Blue dotted line shows the amplitude of state transfer between $| - + \rangle$ and $| + - \rangle$ states. (c) Probability to remain within the hypergrid over time is much higher for $| - + \rangle$ than other states.

growth of entropy at short times is a consequence of the bipartition being located in the middle of a two-site effective cell.

Entropy oscillations mirror those of the wave function return probability, $|\langle\psi_0|e^{-iHt}|\psi_0\rangle|^2$, in Fig. 2(b). For the isolated state $|\downarrow 2 \uparrow\rangle$, only a single revival is clearly visible as the return probability decays rapidly once the wave function leaks out of the tail of the graph. Because of the low connectivity of the tail, the first revival is still visible on the scale of Fig. 2(b). The revival time can be accurately estimated by assuming the tail is completely disconnected, leading to the period $\pi/\sqrt{2}$. In contrast, the state $| - + \rangle$ displays several revivals with the sizable weight of the wave function $\sim 40\%$ returning to its initial value. The fidelity density, $1/N \ln |\langle\psi_0|e^{-iHt}|\psi_0\rangle|^2$, shown in the inset, converges as $1/N$ to a value of -0.058 . In contrast, the inverse Hilbert space dimension, \mathcal{D}^{-1} , expected for a random state leads to a fidelity density of -0.855 —an order of magnitude higher. The scarred dynamics in this case can be visualized as the state bouncing within the hypergrid between $| - + \rangle$ and its partner $| + - \rangle$, illustrated by the dotted line in Fig. 2(b). From the hypergrid analysis, we expect the revival period to be $\sqrt{2}\pi$, coming from the 2π

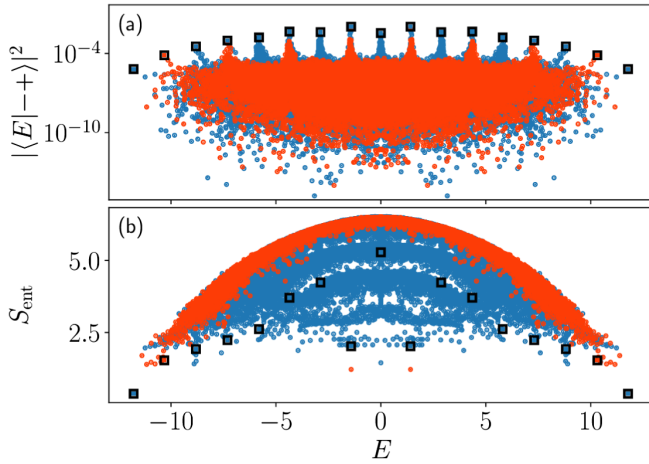


FIG. 3. Eigenstate properties of the effective model Eq. (2). (a) Overlap of eigenstates with the $| - + \rangle$ state as a function of their energy E . (b) Entanglement entropy S_{ent} of the eigenstates. Data is for system size $N = 16$. Red dots correspond to eigenstates with total spin $S = 1$, while the blue ones mark all other spin values. The squares indicate the eigenstates sitting at the top of each tower of states. These towers have an energy separation of approximately $\sqrt{2}$, as expected for the spin-1 hypergrid.

period of free precession and the spin-1 matrix elements $\sqrt{2}$. This prediction closely matches the revival period observed in Fig. 2(b).

The importance of the hypergrid for scarred dynamics is illustrated in Fig. 2(c) which plots the probability to remain in the hypergrid, $P_{\text{HG}}(t) = \langle \psi_0 | e^{i\hat{H}t} \hat{P}_{\text{HG}} e^{-i\hat{H}t} | \psi_0 \rangle$, where \hat{P}_{HG} is the projector onto the subspace spanned by product states belonging to the hypergrid. For the initial state $| - + \rangle$, we observe that the wave function remains concentrated inside the hypergrid, even at late times. This is in stark contrast with the PXP model which describes a chain of Rydberg atoms in the blockade regime [56], where the wave function spreads across the entire graph by the time it undergoes the first revival. Furthermore, even at the first revival peak the fidelity is lower than P_{HG} . This shows that the wave function does not exactly return to itself but gets more spread even within the hypergrid. Finally, for this initial state after a long time P_{HG} converges to a non-zero value which is higher than expected from the relative size of the hypergrid in the Hilbert space [72], hinting that the subgraph could have additional structure that prevents states from leaking out. The fact that this long-time value is much lower for random states in the hypergrid than for $| - + \rangle$ confirms that this is not simply due to low connectivity between the hypergrid and the rest of the Hilbert space, but that the special eigenstates indeed play an important role.

Properties of eigenstates of the model Eq. (2) are summarized in Fig. 3. The projection of eigenstates onto the $| - + \rangle$ state, shown in panel (a), displays prominent tower structures reminiscent of other scarred models [13,48]. The existence of towers implies that eigenstates tend to

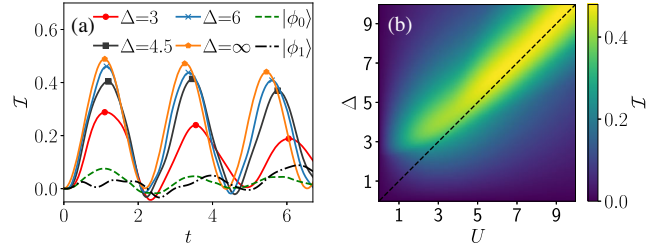


FIG. 4. (a) Occupation imbalance in the full model [in Eq. (1)] with $N = 12$ for various values of $U = \Delta$ for the initial state $| - + \rangle$, and for $U = \Delta = 6$ for the initial states $|\phi_0\rangle = |\uparrow\downarrow\uparrow\downarrow \cdots \uparrow\downarrow\rangle$ (within the hypergrid) and $|\phi_1\rangle = |\downarrow\uparrow\downarrow\uparrow\downarrow\uparrow\downarrow\uparrow\downarrow\rangle$ (outside of it). (b) $U - \Delta$ phase diagram showing the scarring regime near the diagonal (dashed line). The colour scale represents the value of the first peak of the imbalance for $N = 12$.

concentrate around certain energies in the spectrum, causing an ETH violation. The separation between the towers is approximately $\Delta E \approx \sqrt{2}$, as expected from the embedded hypergrid. Note that the eigenstates have been classified according to the conserved total value of spin S ; in contrast, the $| - + \rangle$ state is not an eigenstate of \mathbf{S}^2 . One can show that for this state, $\langle \mathbf{S}^2 \rangle = N/2$, thus $| - + \rangle$ is predominantly supported by $S = 1$ and $S = 2$ eigenstates at the given system size. The $S = 1$ eigenstates are indicated by red points in Fig. 3.

Similar violation of the ETH can be seen in the large spread in entanglement entropy of eigenstates in Fig. 3(b), showing that eigenstates of similar energy have very different amounts of entanglement. Part of this spreading, however, can be attributed to the eigenstates belonging to different spin sectors S , giving rise to multiple bands that do not fully overlap at the system size shown in Fig. 3(b) [72]. The distribution of entropy in the $S = 1$ sector [red points in Fig. 3(b)] is relatively narrow apart from two “outliers” shown at energy $E \approx \pm\sqrt{2}$, which sit at the top of the tower for their sector in Fig. 3(a). The states at the top of each tower are indicated by squares, but unlike the PXP model [56] these states are not well separated from other states in the same tower.

Experimental implications.—The effective model studied above is exact for $U = \Delta \rightarrow \infty$. For experimental realizations, it is important to ascertain that the same physics persists for accessible values of U, Δ and that it can be detected using local measurements. We demonstrate this in Fig. 4 for the full model in Eq. (1) focusing on the regime $U, \Delta < 10$. Panel (a) shows the dynamics of imbalance on the even and odd sublattices, $\mathcal{I} = (N_o - N_e)/(N_o + N_e)$, where $N_{e/o}$ is the total number of fermions on the even or odd sites. The imbalance is bounded between -1 and 1 . We see robust oscillations in \mathcal{I} with the frequency matching half the wave function revival frequency in Fig. 2(b). The amplitude of the imbalance revival remains close to the infinite-limit value for $U = \Delta \gtrsim 6$. As further evidence that the hypergrid is the cause of nonergodicity, we devised a local perturbation

which effectively disconnects the hypergrid, leading to the improvement of revivals in the full model [72].

Conclusions and discussion.—We have proposed an experimental realization of quantum many-body scars in the regime $U = \Delta$ of the tilted FH model. We have identified product states $| - + \rangle$, $| + - \rangle$ at filling factor $\nu = 1$ which give rise to scarred dynamics and reveal towers of ergodicity-breaking many-body eigenstates, allowing us to investigate the interplay of many-body scarring with other facets of weak ergodicity breaking such as localization and Hilbert space fragmentation. In addition to the filling factor $\nu = 1$, we have also studied the filling $\nu = 1/2$ used in Ref. [64]. In the latter case, taking the large-tilt limit $\Delta \gg U, J$ and using a Schrieffer-Wolff transformation up to third order, we found analogous signatures of scars [72], provided we neglect the diagonal terms in the effective Hamiltonian. Under these assumptions, the resulting model can be viewed as a spinful generalization of the fractional quantum Hall effect on a thin torus [23]. By contrast, the approach presented here for $\nu = 1$ is considerably simpler as it allows us to conveniently eliminate the undesirable diagonal terms.

Statement of compliance with EPSRC policy framework on research data: This publication is theoretical work that does not require supporting research data.

We acknowledge support by the Leverhulme Trust Research Leadership Award No. RL-2019-015 (Z. P., A. H.), and by EPSRC Grants No. EP/R020612/1 (Z. P.), No. EP/R513258/1 (J.-Y. D.), and No. EP/M50807 X/1 (C. J. T.). A. H. acknowledges funding provided by the Institute of Physics Belgrade, through the grant by the Ministry of Education, Science, and Technological Development of the Republic of Serbia. Part of the numerical simulations were performed at the Scientific Computing Laboratory, National Center of Excellence for the Study of Complex Systems, Institute of Physics Belgrade.

-
- [1] C. Gogolin and J. Eisert, Equilibration, thermalisation, and the emergence of statistical mechanics in closed quantum systems, *Rep. Prog. Phys.* **79**, 056001 (2016).
- [2] R. Nandkishore and D. A. Huse, Many-body localization and thermalization in quantum statistical mechanics, *Annu. Rev. Condens. Matter Phys.* **6**, 15 (2015).
- [3] D. A. Abanin, E. Altman, I. Bloch, and M. Serbyn, Colloquium: Many-body localization, thermalization, and entanglement, *Rev. Mod. Phys.* **91**, 021001 (2019).
- [4] T. Kinoshita, T. Wenger, and D. S. Weiss, A quantum Newton's cradle, *Nature (London)* **440**, 900 (2006).
- [5] M. Schreiber, S. S. Hodgman, P. Bordia, H. P. Lüschen, M. H. Fischer, R. Vosk, E. Altman, U. Schneider, and I. Bloch, Observation of many-body localization of interacting fermions in a quasirandom optical lattice, *Science* **349**, 842 (2015).
- [6] J. Smith, A. Lee, P. Richerme, B. Neyenhuis, P. W. Hess, P. Hauke, M. Heyl, D. A. Huse, and C. Monroe, Many-body localization in a quantum simulator with programmable random disorder, *Nat. Phys.* **12**, 907 (2016).
- [7] B. Chiaro *et al.*, Direct measurement of non-local interactions in the many-body localized phase, [arXiv:1910.06024](https://arxiv.org/abs/1910.06024).
- [8] M. Serbyn, D. A. Abanin, and Z. Papić, Quantum many-body scars and weak breaking of ergodicity, [arXiv:2011.09486](https://arxiv.org/abs/2011.09486).
- [9] D. P. Arovas, Two exact excited states for the $S = 1$ AKLT chain, *Phys. Lett. A* **137**, 431 (1989).
- [10] S. Moudgalya, N. Regnault, and B. A. Bernevig, Entanglement of exact excited states of Affleck-Kennedy-Lieb-Tasaki models: Exact results, many-body scars, and violation of the strong eigenstate thermalization hypothesis, *Phys. Rev. B* **98**, 235156 (2018).
- [11] M. Schechter and T. Iadecola, Weak Ergodicity Breaking and Quantum Many-Body Scars in Spin-1 XY Magnets, *Phys. Rev. Lett.* **123**, 147201 (2019).
- [12] T. Iadecola and M. Schechter, Quantum many-body scar states with emergent kinetic constraints and finite-entanglement revivals, *Phys. Rev. B* **101**, 024306 (2020).
- [13] K. Bull, I. Martin, and Z. Papić, Systematic Construction of Scarred Many-Body Dynamics in 1D Lattice Models, *Phys. Rev. Lett.* **123**, 030601 (2019).
- [14] S. Chattopadhyay, H. Pichler, M. D. Lukin, and W. Wei Ho, Quantum many-body scars from virtual entangled pairs, *Phys. Rev. B* **101**, 174308 (2020).
- [15] N. Shibata, N. Yoshioka, and H. Katsura, Onsager's Scars in Disordered Spin Chains, *Phys. Rev. Lett.* **124**, 180604 (2020).
- [16] S. Moudgalya, E. O'Brien, B. A. Bernevig, P. Fendley, and N. Regnault, Large classes of quantum scarred Hamiltonians from matrix product states, *Phys. Rev. B* **102**, 085120 (2020).
- [17] F. Maria Surace, G. Giudici, and M. Dalmonte, Weak-ergodicity-breaking via lattice supersymmetry, *Quantum* **4**, 339 (2020).
- [18] Y. Kuno, T. Mizoguchi, and Y. Hatsugai, Flat band quantum scar, *Phys. Rev. B* **102**, 241115(R) (2020).
- [19] O. Vafek, N. Regnault, and B. Andrei Bernevig, Entanglement of exact excited eigenstates of the Hubbard model in arbitrary dimension, *SciPost Phys.* **3**, 043 (2017).
- [20] D. K. Mark, C.-J. Lin, and O. I. Motrunich, Unified structure for exact towers of scar states in the Affleck-Kennedy-Lieb-Tasaki and other models, *Phys. Rev. B* **101**, 195131 (2020).
- [21] D. K. Mark and O. I. Motrunich, η -pairing states as true scars in an extended Hubbard model, *Phys. Rev. B* **102**, 075132 (2020).
- [22] S. Moudgalya, N. Regnault, and B. A. Bernevig, η -pairing in Hubbard models: From spectrum generating algebras to quantum many-body scars, *Phys. Rev. B* **102**, 085140 (2020).
- [23] S. Moudgalya, B. A. Bernevig, and N. Regnault, Quantum many-body scars in a Landau level on a thin torus, *Phys. Rev. B* **102**, 195150 (2020).
- [24] A. Hudomal, I. Vasić, N. Regnault, and Z. Papić, Quantum scars of bosons with correlated hopping, *Commun. Phys.* **3**, 99 (2020).
- [25] H. Zhao, J. Vovrosh, F. Mintert, and J. Knolle, Quantum Many-Body Scars in Optical Lattices, *Phys. Rev. Lett.* **124**, 160604 (2020).

- [26] K. Lee, R. Melendrez, A. Pal, and H. J. Changlani, Exact three-colored quantum scars from geometric frustration, *Phys. Rev. B* **101**, 241111(R) (2020).
- [27] P. A. McClarty, M. Haque, A. Sen, and J. Richter, Disorder-free localization and many-body quantum scars from magnetic frustration, *Phys. Rev. B* **102**, 224303 (2020).
- [28] S. Ok, K. Choo, C. Mudry, C. Castelnovo, C. Chamon, and T. Neupert, Topological many-body scar states in dimensions one, two, and three, *Phys. Rev. Research* **1**, 033144 (2019).
- [29] J. Wildeboer, A. Seidel, N. S. Srivatsa, A. E. B. Nielsen, and O. Erten, Topological quantum many-body scars in quantum dimer models on the kagome lattice, [arXiv:2009.00022](https://arxiv.org/abs/2009.00022).
- [30] B. Buča, J. Tindall, and D. Jaksch, Non-stationary coherent quantum many-body dynamics through dissipation, *Nat. Commun.* **10**, 1730 (2019).
- [31] J. Tindall, B. Buča, J. R. Coulthard, and D. Jaksch, Heating-Induced Long-Range η Pairing in the Hubbard Model, *Phys. Rev. Lett.* **123**, 030603 (2019).
- [32] S. Sugiura, T. Kuwahara, and K. Saito, Many-body scar state intrinsic to periodically driven system, *Phys. Rev. Research* **3**, L012010 (2021).
- [33] K. Mizuta, K. Takasan, and N. Kawakami, Exact Floquet quantum many-body scars under Rydberg blockade, *Phys. Rev. Research* **2**, 033284 (2020).
- [34] B. Mukherjee, S. Nandy, A. Sen, D. Sen, and K. Sengupta, Collapse and revival of quantum many-body scars via Floquet engineering, *Phys. Rev. B* **101**, 245107 (2020).
- [35] N. Shiraishi and T. Mori, Systematic Construction of Counterexamples to the Eigenstate Thermalization Hypothesis, *Phys. Rev. Lett.* **119**, 030601 (2017).
- [36] K. Pakrouski, P. N. Pallegar, F. K. Popov, and I. R. Klebanov, Many-Body Scars as a Group Invariant Sector of Hilbert Space, *Phys. Rev. Lett.* **125**, 230602 (2020).
- [37] J. Ren, C. Liang, and C. Fang, Quasi-Symmetry Groups and Many-Body Scar Dynamics, *Phys. Rev. Lett.* **126**, 120604 (2021).
- [38] N. O’Dea, F. Burnell, A. Chandran, and V. Khemani, From tunnels to towers: Quantum scars from Lie algebras and q -deformed Lie algebras, *Phys. Rev. Research* **2**, 043305 (2020).
- [39] E. J. Heller, Bound-State Eigenfunctions of Classically Chaotic Hamiltonian Systems: Scars of Periodic Orbits, *Phys. Rev. Lett.* **53**, 1515 (1984).
- [40] E. J. Heller, Wavepacket dynamics and quantum chaos, in *Chaos and Quantum Physics*, Vol. 52 (North-Holland, Amsterdam, 1991).
- [41] G. G. de Polavieja, F. Borondo, and R. M. Benito, Scars in Groups of Eigenstates in a Classically Chaotic System, *Phys. Rev. Lett.* **73**, 1613 (1994).
- [42] D. A. Wisniacki, F. Borondo, E. Vergini, and R. M. Benito, Localization properties of groups of eigenstates in chaotic systems, *Phys. Rev. E* **63**, 066220 (2001).
- [43] S. Sridhar, Experimental Observation of Scarred Eigenfunctions of Chaotic Microwave Cavities, *Phys. Rev. Lett.* **67**, 785 (1991).
- [44] P. B. Wilkinson, T. M. Fromhold, L. Eaves, F. W. Sheard, N. Miura, and T. Takamasu, Observation of ‘scarred’ wavefunctions in a quantum well with chaotic electron dynamics, *Nature (London)* **380**, 608 (1996).
- [45] D. Wintgen and A. Hönl, Irregular Wave Functions of a Hydrogen Atom in a Uniform Magnetic Field, *Phys. Rev. Lett.* **63**, 1467 (1989).
- [46] F. J. Arranz, F. Borondo, and R. M. Benito, Scar Formation at the Edge of the Chaotic Region, *Phys. Rev. Lett.* **80**, 944 (1998).
- [47] H. Bernien, S. Schwartz, A. Keesling, H. Levine, A. Omran, H. Pichler, S. Choi, A. S. Zibrov, M. Endres, M. Greiner, V. Vuletic, and M. D. Lukin, Probing many-body dynamics on a 51-atom quantum simulator, *Nature (London)* **551**, 579 (2017).
- [48] C. J. Turner, A. A. Michailidis, D. A. Abanin, M. Serbyn, and Z. Papić, Weak ergodicity breaking from quantum many-body scars, *Nat. Phys.* **14**, 745 (2018).
- [49] W. Wei Ho, S. Choi, H. Pichler, and M. D. Lukin, Periodic Orbits, Entanglement, and Quantum Many-Body Scars in Constrained Models: Matrix Product State Approach, *Phys. Rev. Lett.* **122**, 040603 (2019).
- [50] C. J. Turner, J.-Y. Desaulles, K. Bull, and Z. Papić, Correspondence Principle for Many-Body Scars in Ultracold Rydberg Atoms, *Phys. Rev. X* **11**, 021021 (2021).
- [51] S. Choi, C. J. Turner, H. Pichler, W. Wei Ho, A. A. Michailidis, Z. Papić, M. Serbyn, M. D. Lukin, and D. A. Abanin, Emergent SU(2) Dynamics and Perfect Quantum Many-Body Scars, *Phys. Rev. Lett.* **122**, 220603 (2019).
- [52] K. Bull, J.-Y. Desaulles, and Z. Papić, Quantum scars as embeddings of weakly broken Lie algebra representations, *Phys. Rev. B* **101**, 165139 (2020).
- [53] A. A. Michailidis, C. J. Turner, Z. Papić, D. A. Abanin, and M. Serbyn, Stabilizing two-dimensional quantum scars by deformation and synchronization, *Phys. Rev. Research* **2**, 022065(R) (2020).
- [54] C.-J. Lin, V. Calvera, and T. H. Hsieh, Quantum many-body scar states in two-dimensional Rydberg atom arrays, *Phys. Rev. B* **101**, 220304(R) (2020).
- [55] D. Bluvstein, A. Omran, H. Levine, A. Keesling, G. Semeghini, S. Ebadi, T. T. Wang, A. A. Michailidis, N. Maskara, W. Wei Ho, S. Choi, M. Serbyn, M. Greiner, V. Vuletic, and M. D. Lukin, Controlling quantum many-body dynamics in driven Rydberg atom arrays, *Science* **371**, 1355 (2021).
- [56] C. J. Turner, A. A. Michailidis, D. A. Abanin, M. Serbyn, and Z. Papić, Quantum scarred eigenstates in a Rydberg atom chain: Entanglement, breakdown of thermalization, and stability to perturbations, *Phys. Rev. B* **98**, 155134 (2018).
- [57] V. Khemani, C. R. Laumann, and A. Chandran, Signatures of integrability in the dynamics of Rydberg-blockaded chains, *Phys. Rev. B* **99**, 161101(R) (2019).
- [58] C.-J. Lin, A. Chandran, and O. I. Motrunich, Slow thermalization of exact quantum many-body scar states under perturbations, *Phys. Rev. Research* **2**, 033044 (2020).
- [59] I. Mondragon-Shem, M. G. Vavilov, and I. Martin, The fate of quantum many-body scars in the presence of disorder, [arXiv:2010.10535](https://arxiv.org/abs/2010.10535).
- [60] V. Khemani, M. Hermele, and R. Nandkishore, Localization from Hilbert space shattering: From theory to physical realizations, *Phys. Rev. B* **101**, 174204 (2020).
- [61] S. Pai and M. Pretko, Dynamical Scar States in Driven Fracton Systems, *Phys. Rev. Lett.* **123**, 136401 (2019).

- [62] S. Moudgalya, A. Prem, R. Nandkishore, N. Regnault, and B. A. Bernevig, Thermalization and its absence within Krylov subspaces of a constrained Hamiltonian, [arXiv:1910.14048](https://arxiv.org/abs/1910.14048).
- [63] P. Sala, T. Rakovszky, R. Verresen, M. Knap, and F. Pollmann, Ergodicity Breaking Arising from Hilbert Space Fragmentation in Dipole-Conserving Hamiltonians, *Phys. Rev. X* **10**, 011047 (2020).
- [64] S. Scherg, T. Kohlert, P. Sala, F. Pollmann, Bharath H M, I. Bloch, and M. Aidelsburger, Observing non-ergodicity due to kinetic constraints in tilted Fermi-Hubbard chains, [arXiv:2010.12965v1](https://arxiv.org/abs/2010.12965v1).
- [65] M. Schulz, C. A. Hooley, R. Moessner, and F. Pollmann, Stark Many-Body Localization, *Phys. Rev. Lett.* **122**, 040606 (2019).
- [66] E. van Nieuwenburg, Y. Baum, and G. Refael, From Bloch oscillations to many-body localization in clean interacting systems, *Proc. Natl. Acad. Sci. U.S.A.* **116**, 9269 (2019).
- [67] R. Yao and J. Zakrzewski, Many-body localization of bosons in an optical lattice: Dynamics in disorder-free potentials, *Phys. Rev. B* **102**, 104203 (2020).
- [68] J. M. Deutsch, Quantum statistical mechanics in a closed system, *Phys. Rev. A* **43**, 2046 (1991).
- [69] M. Srednicki, Chaos and quantum thermalization, *Phys. Rev. E* **50**, 888 (1994).
- [70] S. Bravyi, D. P. DiVincenzo, and D. Loss, Schrieffer-Wolff transformation for quantum many-body systems, *Ann. Phys. (Amsterdam)* **326**, 2793 (2011).
- [71] F. H. L. Essler, H. Frahm, F. Göhmann, A. Klümper, and V. E. Korepin, *The One-Dimensional Hubbard Model* (Cambridge University Press, Cambridge, England, 2005).
- [72] See Supplemental Material at <http://link.aps.org/supplemental/10.1103/PhysRevLett.126.210601> for additional details on symmetries of the model and on the effect of the hypergrid on the Hilbert space.
- [73] V. Oganesyan and D. A. Huse, Localization of interacting fermions at high temperature, *Phys. Rev. B* **75**, 155111 (2007).
- [74] M. Lal Mehta, *Random Matrices* (Elsevier, New York, 2004), Vol. 142.
- [75] N. Pancotti, G. Giudice, J. Ignacio Cirac, J. P. Garrahan, and M. Carmen Bañuls, Quantum East Model: Localization, Nonthermal Eigenstates, and Slow Dynamics, *Phys. Rev. X* **10**, 021051 (2020).